Beam Chopper and RF Kicker Systems for the TR24 Cyclotron Injection Line

M. Pellicioli, J. Schuler, C. Ruescas, C. Haas, U. Goerlach, and M. Rousseau
IPHC, UNISTRA, CNRS, 23 rue du Loess, 67200 Strasbourg, France

Corresponding author: M. Pellicioli
Email: michel.pellicioli@iphc.cnrs.fr

Abstract

The ability to switch ion beams on and off quickly is a key point in proton therapy that can be achieved by means of electrical actions. A beam chopper system has first been developed to fulfill this function on the TR24 Cyclotron of the Cyrcé Platform at the IPHC Laboratory. In addition, the capability of discarding one ion beam bunch over two is of great interest in the context of the CMS (Compact Muon Solenoid) detector as it allows us to make tests close to the LHC (Large Hadron Collider at CERN) bunch repetition rate (40 MHz), the cyclotron RF frequency being 85.085 MHz. A second kicker (the so-called RF kicker) has been developed and installed in place of the first one to fulfill both requirements. This article discusses the sizing and characteristics of these two systems that were consecutively installed on the injection line of the TR24 cyclotron. The first system reported uses fast static high-voltage switches while the second one uses an RF resonator to either populate or depopulate the phase acceptance of the cyclotron. To our knowledge, this second system used in this specific context has not yet been reported in the literature.

Keywords: radiobiology, beam switch, kicker, chopper, dose deposition
DOI: 10.31526/JAIS.2023.313

1. INTRODUCTION

Ion beam switches have been addressed in several ways in the past, depending on the intended application. In proton therapy, magnetic switches are commonly used to deflect the beam after acceleration [1, 2]. Magnetic deflectors installed in the high-energy sections allow the beam to be switched in less than 100 μs. The space required is usually several meters to move the beam off its axis. Other applications, like radiolysis for instance, requiring a special beam timing structure (PWM type), have also been reported [3, 4]. Using electrostatic deflectors, these systems are typically installed in low-energy sections and provide beam cut-off in the μs range or less [5]. This makes them very useful for radiobiology applications where dose deposition may require very fast beam bursts.

This area of research is addressed by the Institut Pluridisciplinaire Hubert Curien (IPHC/CNRS) in Strasbourg with a TR24 cyclotron manufactured by ACSI [6] that is part of the research facility called Cyrcé. The TR24 delivers proton beams at energies between 16 and 25 MeV with intensities up to 500 μA [7]. It has two mobile extraction probes for energy selection and an external ion source.

The irradiation applications driven at the Cyrcé are of three types and cover radiobiology applications, sensor characterization, and radiation testing of silicon detectors. These applications require different proton beam characteristics.

In radiobiology, it is essential to be able to deliver known doses that are determined by the beam intensity and the irradiation time. Doses ranging from 1 to 30 Gy can be delivered with beam currents in the range of ten to several tens of pA, typical dose rates between 2 and 15 Gy/min, and irradiation times in the range of half a minute to several minutes. For higher dose rates, up to 1 kGy/s, a much shorter delivery time is required and the time resolution should be of the order of 10^{-4} to 10^{-5} s.

To test the sensors and electronics in the CMS experiment [8] (CMS stands for Compact Muon Solenoid, one of the major LHC experiments at CERN), stable beams of very low intensity, in the range of fA (femtoampere) to a few hundred fA, are required for several hours. Basically, proton beams are used to characterize sensors that are inserted between several reference layers for track reconstruction.

The final area of application is the radiation resistance testing of electronic devices. The current used is in the range of one hundred nA for these applications, and precise knowledge of the deposited doses is required. The doses in this context are of the order of a few tens of kGy. A precise irradiation time is also necessary.

This paper presents the development of two beam kickers consecutively installed in the injection line of the TR24. The first one was a beam chopper on which a high voltage was commuted by means of a fast switch. This fast chopper was developed to control the time of irradiation of underskin tumors of mice with proton beams in the scope of the RPPET project [9] funded by the French National Institute of Cancer (INCA) [10].

The second device called the RF kicker currently in operation uses also two deflectors located in the injection line of the cyclotron, to which an RF high voltage at a quarter of the cyclotron frequency (85.085 MHz) is applied. The motivation for this kicker came from the idea of rejecting every second bunch in order to approach the LHC bunch repetition rate (40 MHz).

If an adequate phase between the two RF signals (see Figure 7) is provided, one bunch over two is accelerated and the other is deflected. Shifting the phase by 45°, all bunches are deflected, thus switching the beam off.

In the first mode, the RF kicker is able to deliver beam bunches at 42.5425 MHz, and in the second mode, the beam is switched off almost completely. The use of a phase jump on the deflector RF signal to switch the beam on and off is an original feature rarely used in such a device.

This equipment has been funded by the CMS collaboration and is commonly used either for sensor testing or for accurate timing in the scope of dose delivery.

2. MATERIAL AND METHODS

2.1. Description of the Research Infrastructure

The former building of a decommissioned tandem accelerator was reused to install the cyclotron, the irradiation area, and the chemistry laboratories of the Cyrcé infrastructure [11]. It consists of a 2 m thick concrete vault for isotope production and a recently added irradiation area. This zone was financed by the PRECy project of the State-Region Project Contract (CPER), the objective of which is to develop a facility for radiobiological experiments [12]. It was designed to accommodate up to five beamlines, two of which are now fully operational. The first beamline is dedicated to radiobiological applications and the second, funded by the CMS collaboration, is used for sensor testing (see Figure 1).

The TR24 cyclotron is a horizontal machine that requires a combination magnet at the beam exits when transporting the beam over long distances (see Table 1 for the TR24 main features). The beam injection line where the kicker deflectors are installed is vertical and is located under the cyclotron. As the space available in the cyclotron injection line did not allow for the installation of two sets of deflectors, the first system was replaced by the second.

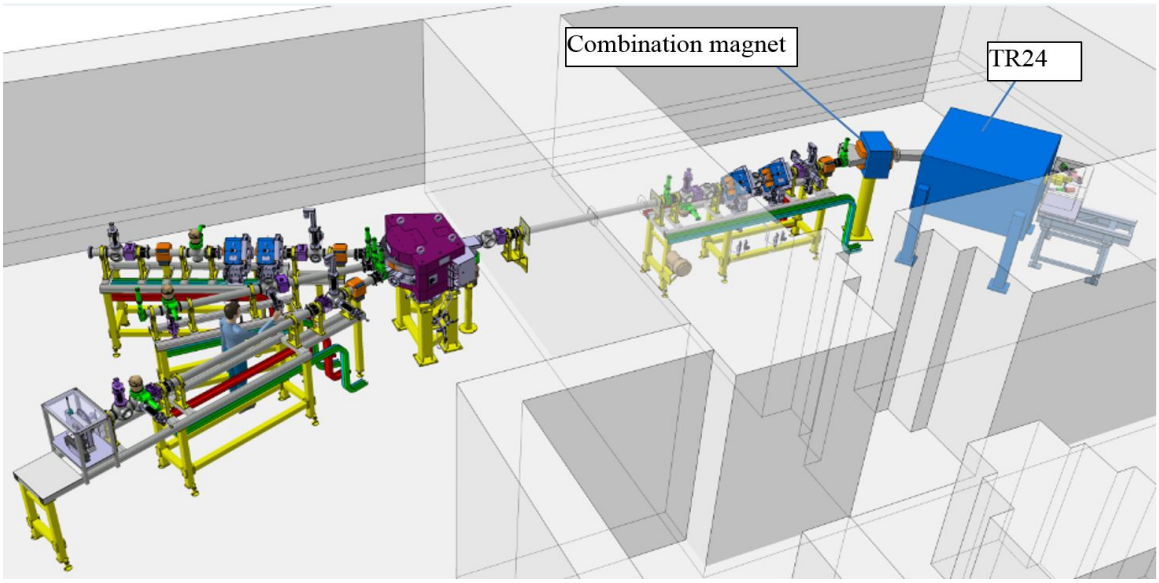

FIGURE 1: 3D modelization of the vault and irradiation area.

Energy range	16 to 25 MeV
Particle	Proton
Beam current	From fA to 500 μA
Ion Source	Cusp, external
Exit ports	2

TABLE 1: Main features of the TR24 cyclotron.

2.2. Beam Deviation

2.2.1. High-Voltage Beam Chopper

The beam energy in the TR24 injection line is 30 keV. A vacuum chamber initially dedicated to a buncher (not installed) was used to install the deflector plates. The size of the beam at the entrance to the chamber is approximately 1 cm in diameter in both the X and Y planes, accompanied by a beam halo with a diameter of approximately 5 cm.

The voltage required to deflect the beam depends on the spacing and length of the plates; the longer and closer they are, the lower the voltage required. However, any collision between the beam and the plates must be avoided; otherwise, a scattered beam may be created, some of which end up in the injection line.

The compromise between these constraints leads to deflection plates of 5.5 cm in length spaced 4.5 cm apart and a voltage of 8 kV max. A 3 cm diameter collimator is added to the end of the chamber to cut off the residual halo of the deflected beam.

The beam deflection at the collimator position is given by equation (1) derived from the application of the fundamental principle of dynamics.

$$y_{d1} = \frac{q}{ml} V * \frac{d_0}{v_z^2} * \left(d_1 - \frac{d_0}{2} \right) + v_{y0} * \frac{d_1}{v_z} + y_0, \tag{1}$$

with

$$v_z = \left(\frac{2E}{m} \right)^{\frac{1}{2}}, \tag{2}$$

where q is the elementary charge, m the proton mass, V the voltage between the plates, l the spacing between the plates, d_0 the length of the plates, d_1 the distance between the plates and the collimator, v_{y0} the initial speed along y axes (transverse axis), y_0 the initial position in the y axis, v_z the proton velocity, and E the beam energy.

Figure 2 shows the deflection of a 2 cm diameter beam (the red lines are only intended to visualize the central area of the beam).

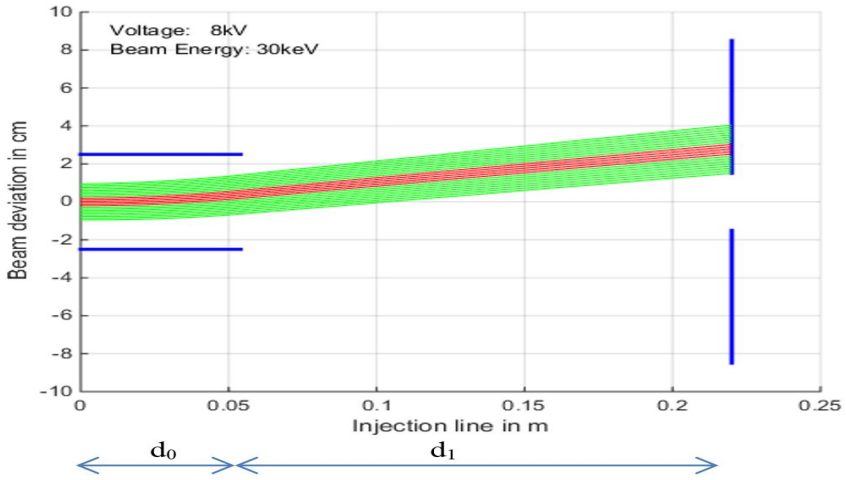

FIGURE 2: Calculated beam deviation.

2.2.2. RF Kicker

The kicker RF frequency is chosen at 21.27125 MHz, the fourth of the cyclotron frequency.

The optimal length of the deflectors is equal to the distance traveled by the protons during half the period of the kicker RF frequency and depends then on the beam energy and the kicker frequency (equation (3))

$$L_{\text{opt}} = \frac{v_z}{2 * f_{\text{kicker}}} = 54{,}5\,\text{mm}. \tag{3}$$

The application of the fundamental principle of dynamics leads to equation (4) for the beam deflection:

$$\begin{aligned} y(z) = y_0 + \frac{z}{v_z} * \left(v_{y0} + \frac{q}{ml\omega} V_{\max} \cos(\varphi) \right) \\ - \frac{q}{ml\omega^2} V_{\max} * \left(\sin\left(\omega * \frac{z}{v_z} + \varphi \right) - \sin(\varphi) \right), \end{aligned} \tag{4}$$

where q is the elementary charge, m the proton mass, $V_{\max}$ the maximum of the RF voltage, l the spacing between the plates, ω the pulsation of the RF voltage, φ the initial phase of the RF voltage, v_{y0} the initial speed along y axes (transverse axis), y_0 the initial position in the y axis, and v_z the proton velocity.

Figure 3 shows the maximum and minimum beam deflections as a function of the phase of the voltage on the deflectors. For a minimum deflection, a beam shift is observed in the *Y* plane.

These simplified calculations do not take into account fringe field effects at the edges of the deflectors, which in any case only increase the desired deflection effect. As the expected performance is achievable with flat deflector profiles, only this type of deflector has been considered in this study. Flat deflectors with chamfered edges were made in the laboratory's mechanical workshop.

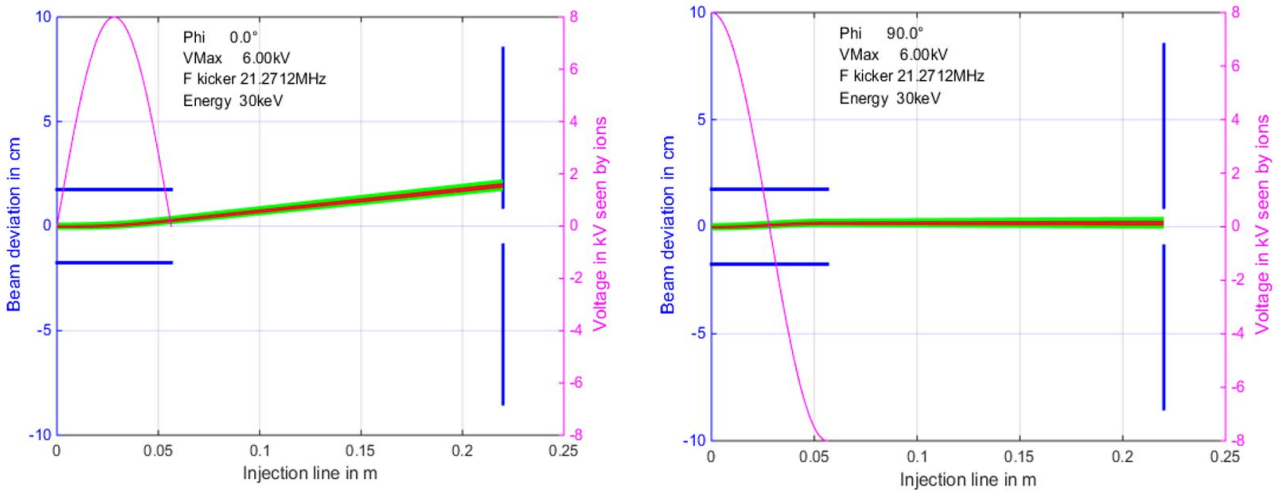

(a) (b)

FIGURE 3: (a) Phase for maximum deviation of the beam. (b) Phase for minimal deviation of the beam (offset into the *Y* plane).

2.3. Development of the High-Voltage Beam Chopper

2.3.1. Synopsis

The chopper uses a high-voltage power supply and a BEHLKE fast switch [13] installed in a compact assembly on the cyclotron injection line.

The principle of operation is as follows: in the resting state, the switch is off, voltage is applied to the deflectors, and the beam is deflected. When the switch is turned on, the voltage is shorted and the beam is restored (see Figure 4).

The Cb capacitors are buffers to maintain the high voltage during the transition between the "On" and "Off" states. The resistors RL and Rd are intended to limit the current through the switch in the "On" state and the discharge current of the capacitors Ck in the switch, respectively. The higher the Rd is, the longer the fall time is. The resistors used are massive, unwired, and also not too compact to avoid sparking between their terminals.

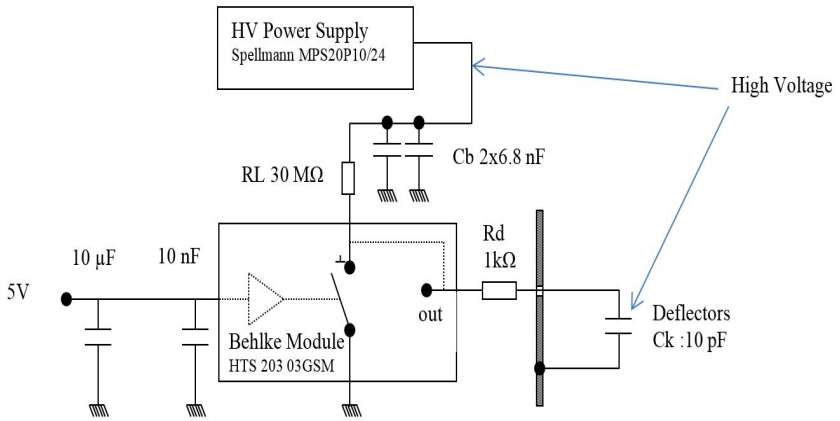

FIGURE 4: Fast high-voltage switch synopsis.

2.3.2. *Implementation and Beam Measurement Setup*

Figure 5 shows the setup used to assess the efficiency of the kicker. A proton beam of approximately 5 pA is collected on a scintillating plastic behind an air outlet of the beam. A photomultiplier allows us to count the protons collected. The residual current is measured when the beam is kicked out. The rejection factor is defined as the ratio between the residual current and the initial beam current.

The rejection factor was measured for different chopper voltages and two sets of collimators.

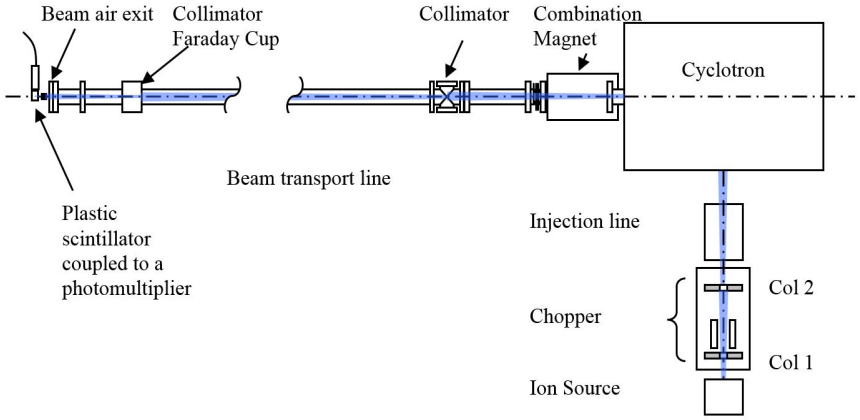

FIGURE 5: Setup use for rejection estimation.

Two collimators located, respectively, 10 mm upstream of the deflectors at the chamber entrance (Col 1) and 220 mm after the first collimator at the chamber exit (Col 2) were used to suppress the beam halo and increase the beam cut-off.

Figure 6(a) shows the vertical injection beam line of the TR24 with the chopper mounted. A high-voltage feedthrough allows high voltage to be applied to one deflector, the other being grounded. Figure 6(b) shows the inside of the chopper box. A discharge rod is installed after the opening to avoid any risk of electric shock.

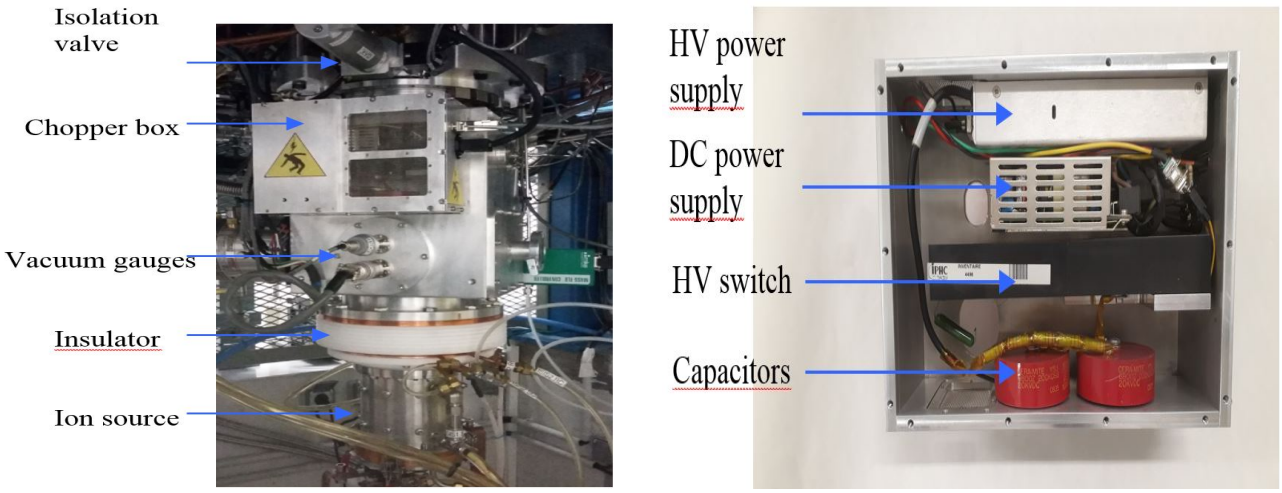

(a) (b)

FIGURE 6: (a) View of the cyclotron injection line with the chopper installed. (b) Inner view of the chopper box.

2.4. *Radio Frequency Kicker*

2.4.1. *Basic Principle*

The TR24 cyclotron has four accelerating gaps on two separated sectors working in phase at a frequency of 85.085 MHz.

According to Figures 7(a) and 7(b), protons entering gap 1 at time t_1 will enter gap 2 at t_2, gap 3 at t_3, etc., and will be accelerated. Protons out of phase (arriving outside the green area) will be discarded. At t_3, a new bunch can be accelerated in gap 1 whereas protons arriving at t_2 on gap 1 will find a reverse voltage and will be lost.

An RF signal at a fourth of the frequency of the cyclotron RF, applied on deflectors in the injection line, may theoretically either discard one bunch over two (Figure 8(a)) or suppress all the bunches (Figure 8(b)), therefore switching the beam off, according to the phase of the RF voltage and provided the voltage is high enough. The green areas represent the phase acceptance of the cyclotron and the red areas show when the kicker voltage is high enough to deflect the beam.

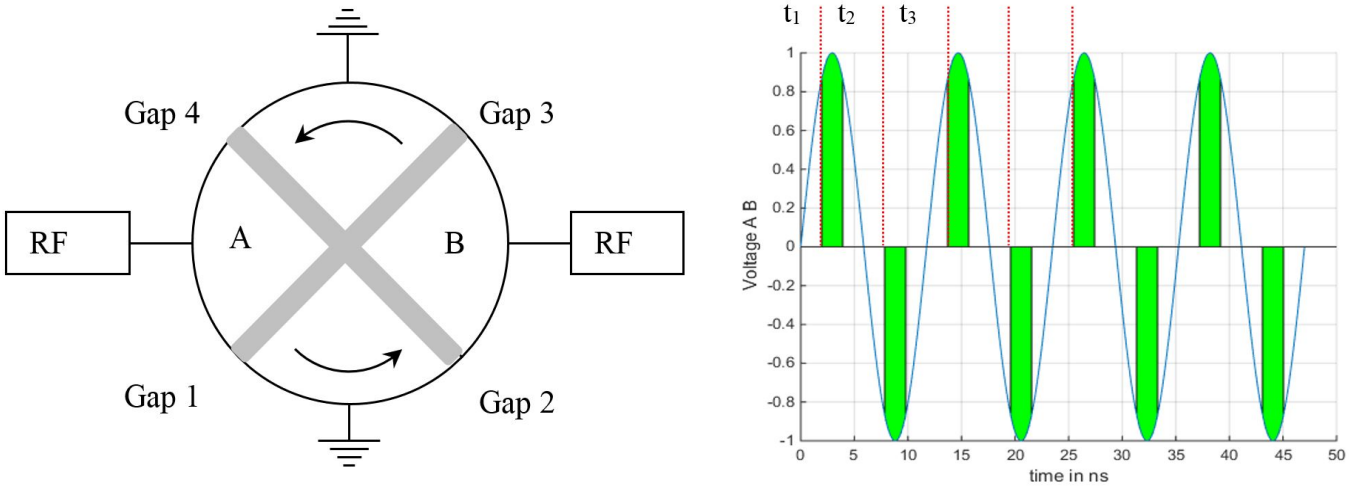

(a) (b)

FIGURE 7: (a) Synopsis of the TR24 cyclotron. (b) RF voltage applied on Dees A and B.

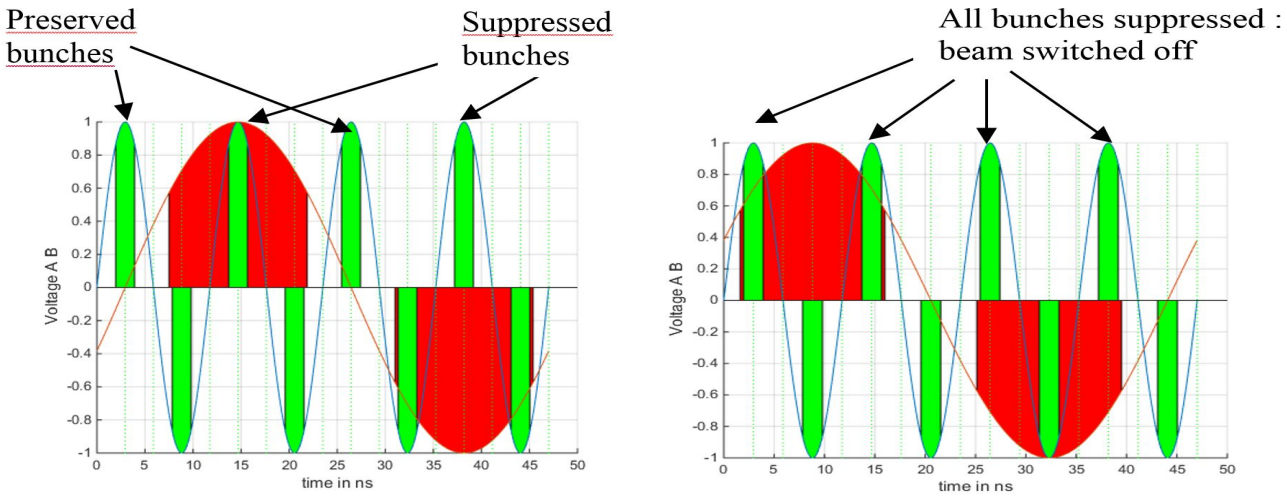

(a) (b)

FIGURE 8: (a) RF kicker phase adjusted to preserve one bunch out of two. (b) RF kicker phase adjusted to suppress all bunches (45° shifted).

2.4.2. Resonant Circuit

An LC resonant circuit tuned to 21.27125 MHz coupled with an exciting coil is used to generate the RF high voltage as shown in Figure 9.

To reduce the effect of the parasitic capacitances, the midpoint of the main coil is grounded. The main parasitic capacitance comes from both feedthroughs that have to hold vacuum, high voltage, and high currents.

The capacitances of the different elements are as in Table 2.

A 15 pF variable capacitor was added to tune the circuit to the resonant frequency. An overall capacitance of 30 pF was therefore considered, bringing the value of the inductor to 1.87 μH.

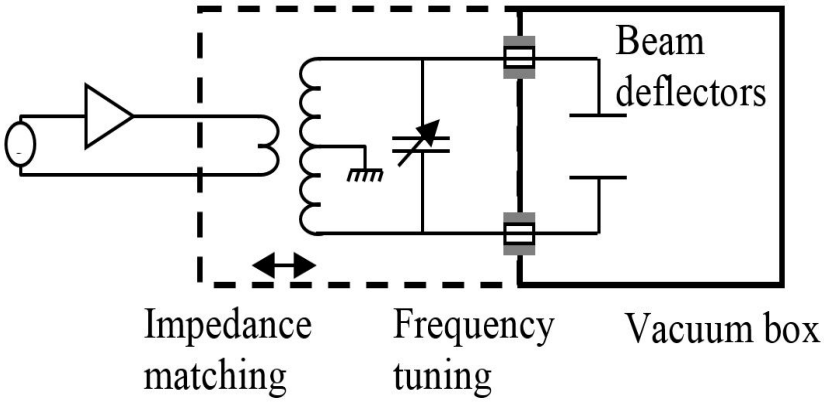

FIGURE 9: RF high-voltage switch synopsis.

Deflectors	<1 pF (calculated)
Deflector vs vacuum box	<1 pF (estimated)
Feedthrough	10 pF each (measured)
Coil vs box	<1 pF (estimated)

TABLE 2: Capacitance of the different elements of the kicker.

2.4.3. Coil Design

A standard annealed copper plumbing pipe with silver plating was used for the coil. The NAGAOKA [14] formulas were used to optimize the design of the coil.

The main ohmic resistance of the coil is given by the length of the conductor, corrected by a factor that takes into account an additional resistance induced by the tightening of the turns. The quality factor of the coil, which is governed by its resistance, has a maximum for a given inductance value and geometry as shown in Figure 10 (green plot). In practice, the measured Q-factor for the whole circuit is much lower than this optimum value and is around 650 instead of the theoretical value of 3526, due to the additional resistance of the connections and feedthroughs. For the record, the quality factor of a resonant circuit is defined as the total stored energy divided by the energy loss at each RF cycle, times $2^{*}\Pi$. Q can be expressed by equation (5) where L is the inductance L of the coil and R is the resistance of the resonant circuit.

$$Q = \frac{L\omega}{R}. \tag{5}$$

The red, blue, and magenta plots of Figure 10 show, respectively, the height of the coil, its diameter, and its resistance according to the number of turns of the coil.

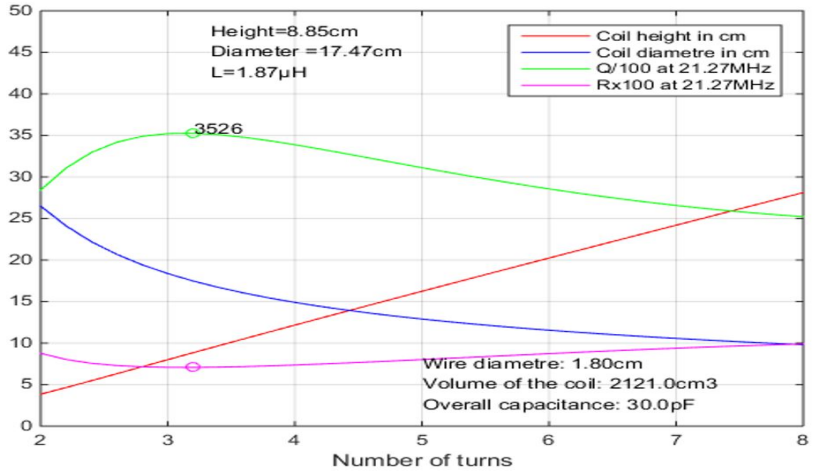

FIGURE 10: Quality factor versus the number of turns.

According to the skin effect at 21.27125 MHz, a 13 μm silver layer was applied to the coil.

Figure 11 shows the coil after electroplating with 6 PEEK supports "screwed" into the coil in order to maintain its geometry (PEEK means Polyether ether ketone which is an organic thermoplastic polymer).

FIGURE 11: Silver-coated coil.

2.4.4. Implementation in the Beam Injection Line

Figure 12 shows the mechanical design of the whole system and Figure 13 shows the installation in the injection line. The coil is inserted into a box containing the tuning capacitor, the excitation coil, and the two electrical feedthroughs. The vacuum box contains the deflectors and a set of two removable collimators. Two actuators allow fine-tuning and matching of the resonant circuit. A third actuator is used to insert or remove the collimators.

The downstream and upstream apertures of the collimators have a diameter of 12 and 8 mm, respectively. To reduce beam scattering, cone-shaped collimators have been designed as shown in Figure 12. A negative voltage may be applied to the collimators to increase the rejection rate (see Section 4.2).

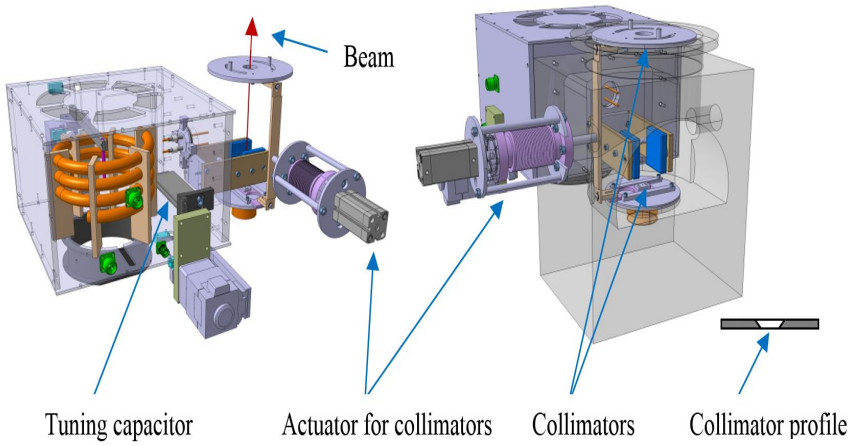

FIGURE 12: View of the entire mechanical assembly.

The electrical connections were made with large silver foils screwed or soldered (especially on the feedthrough) to reduce the overall resistance of the circuit to a minimum.

Table 3 shows that it is possible to achieve a maximum voltage of about 6 kV with an RF power of 100 W. This leads to a reasonable current in the resonator and in particular in the feedthroughs which are designed to withstand 100 A.

2.4.5. Power Amplifier and Electronic Control

The power required to drive the resonant circuit is derived from the following equation:

$$P = \frac{1}{2}\frac{L\omega}{Q} I_{\max}^2 = \frac{1}{2}\frac{C\omega}{Q} U_{\max}^2. \tag{6}$$

The higher the Q-factor, the lower the power required for a given $U_{\max}$ value. A 250 W power amplifier from RFPA was purchased for this application [15].

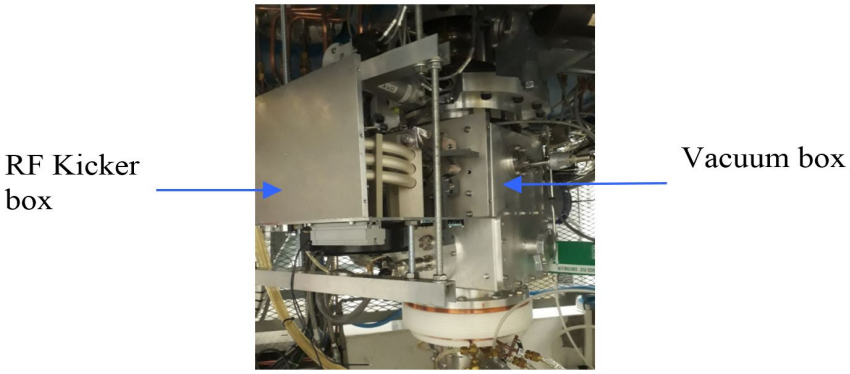

FIGURE 13: View of the RF kicker box opened.

Power (W)	15	60	80	100
U_{max} (kV)	2.2	4.4	5.1	5.7
I_{max} (A)	8.8	17.7	20.4	22.8

TABLE 3: Calculated voltage and current on the resonant circuit versus RF power (Q-factor = 650).

The schematic of the electronic is given in Figure 14 and its realization in Figure 15. It is composed of the following:

(i) An RF synthesizer (HMS 1001) locked to the cyclotron synthesizer set to 21.27125 MHz. Its level is set at 6.8 dBm and its phase is adjusted by the PLC to optimize the beam current.

(ii) A passive 50 Ω splitter (A).

(iii) A programmable attenuator (from 0 to 31.5 dB by step of 0.5 dB).

(iv) A phase shifter consisting of a splitter and an RF SPDT switch. An extra length of cable on one of the paths allows the addition of a phase shift to turn the beam on and off.

(v) A passband filter to reject harmonics.

(vi) A fixed 20 dB gain amplifier.

(vii) The power amplifier from RFPA (53 dB 250 W) equipped with forward and reflected power measurements. The line between the power amplifier and the resonator is a 10 m long 50 Ω power cable that crosses the 2 m vault wall.

In the case of resonator settings, a network analyzer is connected instead of the amplifier. On the lower part, we have another splitter that allows the distribution of two RF signals.

(viii) Another splitter (B) allows the distribution of two RF signals.

(ix) The first is connected to a phase comparator that gives an error signal with an RF pickup signal from the resonator. When matched, the resonator signal is in phase with the input signal. The difference can be used to automatically adjust the tuning to maintain optimum tuning.

(x) The second one is used to produce a reference signal at twice the frequency (bunch frequency) delivered to the experimental area.

3. RESULT

3.1. Beam Chopper

The rejection factor for two sets of collimators and the switching time have been evaluated.

The characteristics of the two sets of collimators are given in Table 4.

Figure 16 shows beam cut-off occurring at voltages in the 2-3 kV range, with virtually no improvement at higher voltages, regardless of the setup used.

At the time of the experiment, the upper limit of the kicker's switching capacity was established as being better than 100 μs, this being the refresh latency of a CMOS sensor used to evaluate this parameter.

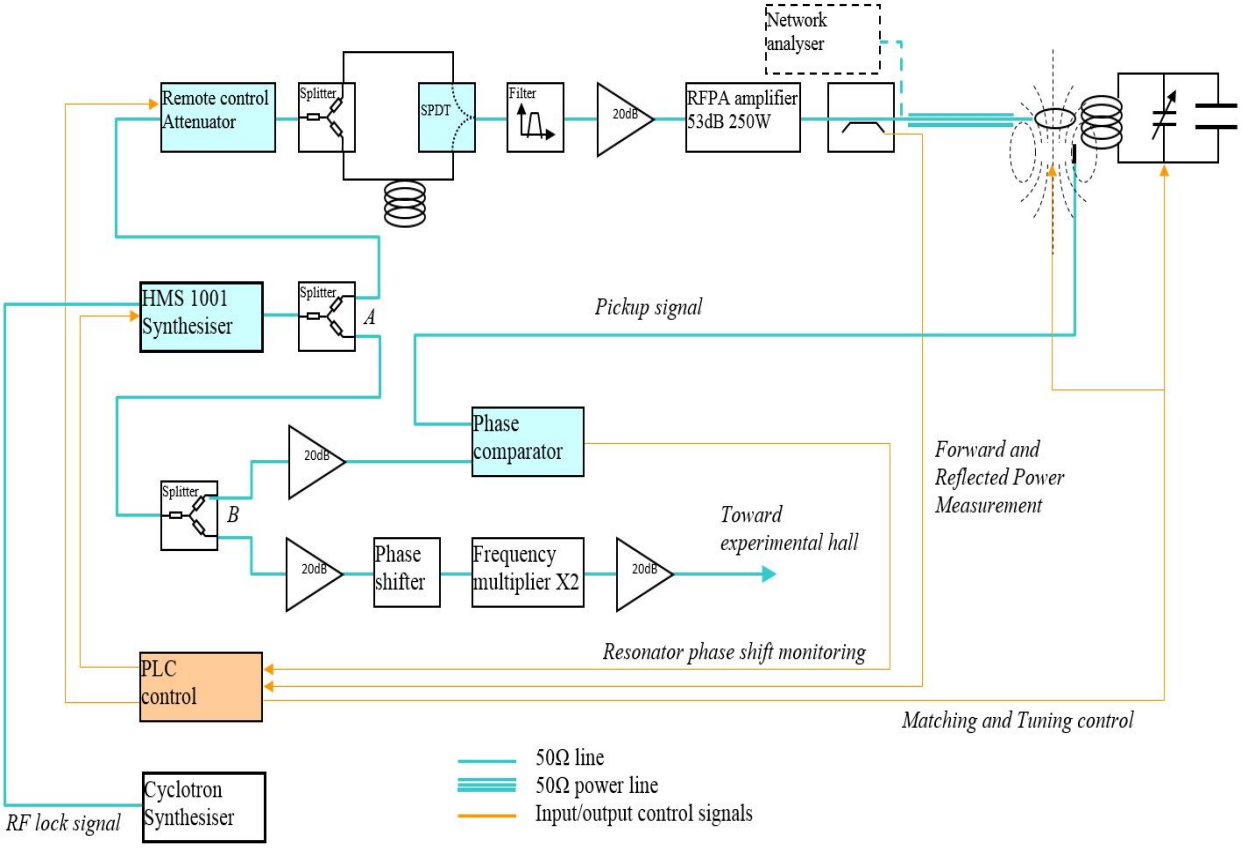

FIGURE 14: Synopsis of the electronic control.

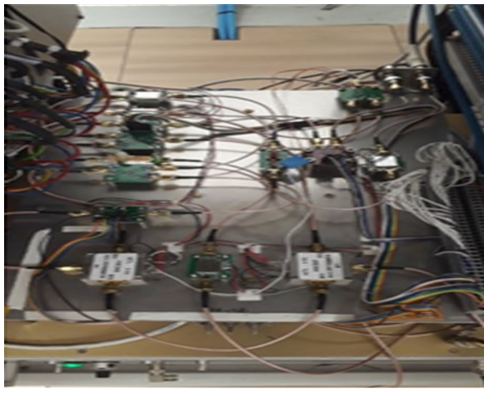

FIGURE 15: Implementation of the electronic control.

Setup	Upstream collimator diameter (mm)	Downstream collimator diameter (mm)
1	49.8	50
2	18.9	30

TABLE 4: Sets of collimators used with the kicker.

3.2. *Radio Frequency Kicker*

Tests have shown that transmitted power above 80 W does not provide any improvement in either mode. This leads to a reasonable current in the resonant circuit and especially in the feedthroughs.

To qualify the first mode, in which every second bunch is discarded, analog scintillators combined with fast electronics were used to quantify the temporal structure of the beam. The beam bunches do arrive at a rate of half the cyclotron frequency, as expected. A beam current of 50 fA was used for this result (see Figure 17).

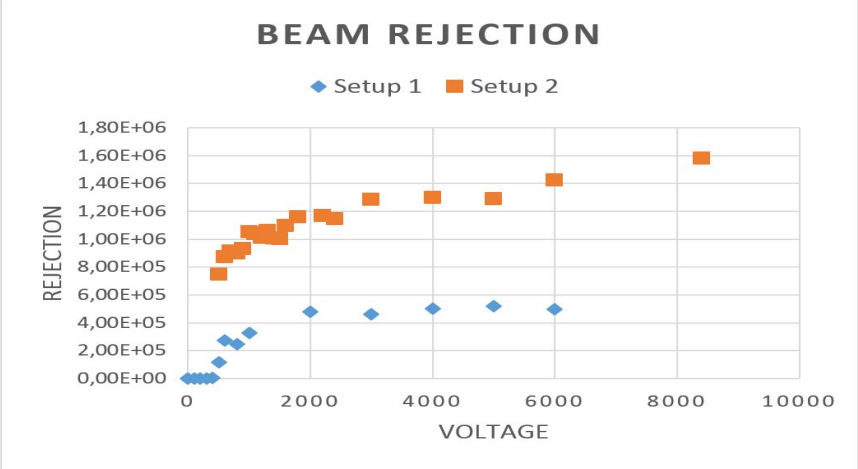

FIGURE 16: Beam rejection for setups 1 and 2 versus the voltage on deflectors.

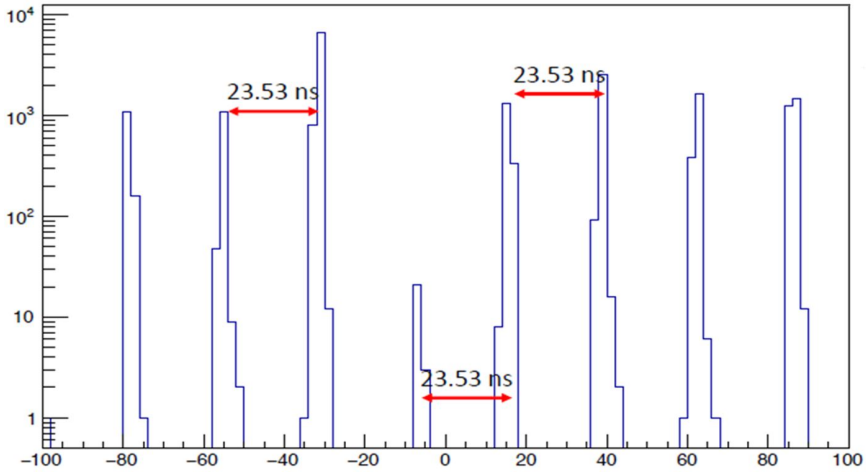

FIGURE 17: Bunches arrival time with RF kicker on.

The second mode was qualified by measuring the rate of beam rejection when a phase jump of the RF kicker signal was applied. The best ratio obtained is around $2.2 \cdot 10^5$ for a beam current of 50 nA, an RF power of 15 W, and -150 V applied on collimators.

Fast acquisition systems have put an upper bound on the switching time of 10 μs, which is more than comfortable for radiobiology applications.

4. DISCUSSION

4.1. Beam Chopper

Although the voltage is sufficient to theoretically remove the entire beam, there is still a residual current regardless of the voltage applied. Fortunately, very high rejection rates can still be achieved.

It can be seen that the rejection rate reaches a plateau for voltages above 2 to 3 kV, and it seems that the smaller the collimators, the worse the rejection, whereas the opposite might have been expected.

This result can be explained by the amount of beam scattered by the edge of the input collimator compared to the beam passing through it. Among all the scattered protons and whatever the voltage, some will have the right angle to pass through the injection line. A solution to this problem of getting the highest rejection rate is to use cone-shaped collimators to minimize beam interactions. This option is used in the RF kicker as described above.

As the intrinsic switching time of Behlke's device is claimed to be of the order of ns, the switching time is likely much better than the observed upper limit, but it was not possible to measure this at the time.

The switching frequency of the beam chopper has not been evaluated in this work. It can only be said that it is driven by the capacitances of the high-voltage switch.

4.2. RF Kicker

While the beam chopper physically cuts off the beam to extinguish it, the RF kicker relies on the temporal structure of the acceleration to reject the beam. This makes a big difference because the beam always enters the cyclotron, whether we want to keep it or reject it. For this reason, the rejection rate has required many efforts to be optimized and is still lower than what can be achieved with the beam chopper. All the elements used to transport the beam on the injection line have an impact on either the rejection rate or the maximum current available and make the adjustment more difficult. Along the injection line and for each setting of the RF kicker, beam optimization requires adjusting bias voltage (which gives injection beam energy), X and Y steerers, quadrupole currents, injection deflector voltage (deflector that guides the beam inside the cyclotron), and even cyclotron main magnet current.

In practice, after power-up, the phase of the synthesizer is adjusted to maximize the beam current. If all line pieces of equipment are adjusted correctly, the application of the phase jump will minimize the beam current. The pickup signal (see Figure 14) that gives an image of the resonator voltage is used to track the phase and amplitude drift of the voltage. The phase drift is compensated by the tuning capacitance and the amplitude is modified by the excitation level.

However, once the set of parameters has been established for a given kicker configuration, it is possible to systematically find more or less the same rejection rate, which can be around $3 \cdot 10^4$ to $10 \cdot 10^4$, making the adjustment very easy. To increase the rejection rate, it is necessary to apply a voltage to the collimators as explained hereinafter.

The choice of the two collimators upstream and downstream of the deflector plates is of primary importance for performance. As mentioned earlier, they are conical in shape to minimize the area of beam interaction with the collimators.

The interaction between the beam and the collimator material can induce two physical effects on the beam ions: deflection and energy loss. Ions deflected by the first edge of the collimator may enter the deflection zone at an angle that could send them back onto the beam axis at a time when they should be removed, adding possible spurious currents. Ions that lose a small amount of energy due to their interaction with a collimator will arrive with a delay between the dees of the cyclotron and could fall into an acceleration phase, thus contributing to increased parasitic currents. Indeed, an ion that loses 1 keV (out of 30) traveling 1 meter would be delayed by 9 ns when the cyclotron RF period is 11.75 ns.

In order to reduce the latter effect, a negative voltage has been applied to the collimators. The sharp edge of the collimator locally induces a high electric field capable of repelling H-ions from the beam, thus limiting collisions with the collimators. The overall effect of this field is null along the longitudinal axis as the ions pass through the collimators, thus avoiding energy loss. The voltage on the collimators is set to -150 V. By applying this voltage, the rejection rate can be more or less doubled.

Another effect induced by this field is to make the collimators behave like Einzel lenses. This effect is compensated by the two magnetic quadrupoles located downstream of the kicker, along the cyclotron injection line.

Different collimator sizes were tested. The first one is used to cut the halo beam and keep its center, and the second one defines the deflection needed to spread the beam. Round shapes of 12 and 8 mm in diameter were chosen for the upstream and downstream collimators.

The RF voltage applied to the deflector plates has an optimum value defined by two effects. On the one hand, the voltage must be sufficient to deflect the entire beam out of the downstream collimator hole. On the other hand, if the voltage is too high, it will greatly reduce the maximum amount of available beam accelerated by the cyclotron due to a shorter voltage zero crossing time. As the stray beam is not greatly affected by the deflection voltage, the optimum value will be the one that keeps as much of the beam as possible while allowing sufficient deflection. This is set at approximately 2.5 kV.

The injection line uses a cryogenic pump that causes vibrations that can slightly detune the resonant circuit whose high-quality factor makes it very sensitive to mechanical changes. This detuning has an impact on the phase and amplitude of the RF voltage. While amplitude variations are more or less acceptable, phase deviations due to vibration should be avoided as they have a direct impact on beam rejection. The cryogenic pump has been mounted on decoupling bellows to avoid this problem.

5. CONCLUSION

Both beam chopper and RF kicker implementations and results have been reported. The beam chopper previously installed offers a high rejection rate and is compact and quite simple to use. It had the disadvantage of being installed inside the vault and had to be removed before each isotope production in order to avoid possible damage to the electronics induced by high neutron flux.

The RF kicker currently installed on the IPHC's TR24 injection line is operating as intended in its two modes, either for radiobiology or for the qualification of CMS detectors. Although the rejection rate of the RF kicker is about an order of magnitude lower than that of the previous device (105 versus 106), it has so far been quite sufficient for all radiobiology applications, especially in flash radiotherapy where typical dose rates of the order of 100 Gy/s are targeted for a delivery time of 100 ms in order to achieve 10 Gy on biological tissues.

Its great advantage over the static kicker is its insensitivity to neutron flux as no sensitive electronics are present inside the vault. The equipment is therefore never removed from the injection line, as was the case with the previous kicker.

CONFLICTS OF INTEREST

The authors declare that there are no conflicts of interest regarding the publication of this paper.

ACKNOWLEDGMENTS

The authors would like to acknowledge the Institut National du Cancer (INCA), which financially supports the development of the static kicker, and the IN2P3, which financially supports the development of the RF kicker for the CMS team. The PRECy project is supported by the Contrat de Projet Etat-Région (CPER) number 918-15 C1, France, Région Grand-Est, 2015–2020, France, and Eurométropole Strasbourg (EMS), France, CNRS, France. The authors would like to thank the researchers who support that project, especially Dr. J. Andrea from the CMS collaboration and Dr. D. Brasse from the molecular imaging department of IPHC, engineers and technicians of the IPHC who worked on these projects, Dominique Thomas, Steve Veeramootoo, and Eddy Dangelser from the mechanical workshop, Fabienne Hamel and Nadine Reinbold from the administration services, and Mr. Russell Watt from ACSI Company for the fruitful discussions we had on that subject.

References

[1] W. Han, X. Liu, B. Qin, and D. Li, "Design considerations of a fast kicker system applied in a proton therapy beamline," Nuclear Instruments and Methods in Physics Research Section A: Accelerators, Spectrometers, Detectors and Associated Equipment, vol. 940, p. 199–205, oct. 2019, doi:10.1016/j.nima.2019.06.034.

[2] E. Dallago, G. Venchi, S. Rossi, M. Pullia, T. Fowler, and M. B. Larsen, "The power supply for the beam chopper magnets of a medical synchrotron," in 2006 37th IEEE Power Electronics Specialists Conference, juin 2006, p. 1–5, doi:10.1109/pesc.2006.1711914.

[3] F. Poirier et al., "The Pulsing Chopper-Based System of the Arronax C70XP Cyclotron," in 10th International Particle Accelerator Conference, Melbourne, Australia, mai 2019, p. TUPTS008, doi:10.18429/JACoW-IPAC2019-TUPTS008.

[4] A. C. Caruso et al., "The LEBT Chopper for the Spiral 2 Project," in Proc. IPAC'11, San Sebastian, Spain, Sep. 2011, paper TUPS082, pp. 1731–1733.

[5] N. R. Lobanov, P. Linardakis, and D. Tempra, "Bunching and chopping for tandem accelerators. Part II: Chopping," Nuclear Instruments and Methods in Physics Research Section B: Beam Interactions with Materials and Atoms, vol. 499, p. 142–147, juill. 2021, doi:10.1016/j.nimb.2021.02.014.

[6] ACSI website: http://www.advancedcyclotron.com/.

[7] P. Marchand, A. Ouadi, M. Pellicioli, and D. Brasse, "Cyrcé, un cyclotron pour la recherche et l'enseignement en Alsace," L'Actualité Chimique, vol. 386, p. 9–14, 2014.https://hal.archives-ouvertes.fr/hal-01059839/.

[8] https://home.cern/fr/science/cms

[9] David Brasse, Hélène Burckel, Patrice Marchand, Marc Rousseau, Ali Ouadi, Marie Vanstalle, Christian Finck, Patrice Laquerriére, and Fréderic Boisson, "Comparison of the [18F]-FDG and [18F]-FLT PET Tracers in the Evaluation of the Preclinical Proton Therapy Response in Hepatocellular Carcinoma," Molecular Imaging and Biology, 62 (2021).

[10] https://www.e-cancer.fr/

[11] E. Bouquerel, E. Traykov, C. Maazouzi, M. Rousseau, M. Pellicioli, T. Adam, P. Graehling, C. Mathieu, G. Heitz, M. Krauth, D. Oster, T. Foehrenbacher, C. Ruescas, J. Schuler, U. Goerlach, and C. Haas, "Design and commissioning of the first two Cyrcé extension beamlines," Nuclear Instruments and Methods in Physics Research Section A: Accelerators, Spectrometers, Detectors and Associated Equipment 1024, 166034 (2022). https://doi.org/10.1016/j.nima.2021.166034

[12] http://www.iphc.cnrs.fr/-PRECy-.html

[13] http://www.behlke.com/

[14] Hantaro Nagaoka, "The Inductance Coefficients of Solenoids", Journal of the College of Science, Imperial University, Tokyo, Vol. 27, Article 6, 1909. http://electronbunker.ca/DL/Nagaoka_1909.pdf

[15] https://www.rfpa.com/